JACS
JOURNAL OF THE AMERICAN CHEMICAL SOCIETY
pubs.acs.org/JACS
Article

Ternary Alloys Enable Efficient Production of Methoxylated Chemicals via Selective Electrocatalytic Hydrogenation of Lignin Monomers

Tao Peng, Taotao Zhuang, Yu Yan, Jin Qian, Graham R. Dick, Jean Behaghel de Bueren, Sung-Fu Hung, Yun Zhang, Ziyun Wang, Joshua Wicks, F. Pelayo Garcia de Arquer, Jehad Abed, Ning Wang, Armin Sedighian Rasouli, Geonhui Lee, Miao Wang, Daping He, Zhe Wang, Zhixiu Liang, Liang Song, Xue Wang, Bin Chen, Adnan Ozden, Yanwei Lum, Wan Ru Leow, Mingchuan Luo, Debora Motta Meira, Alexander H. Ip, Jeremy S. Luterbacher,* Wei Zhao,* and Edward H. Sargent*

Cite This: https://doi.org/10.1021/jacs.1c08348

ABSTRACT: We explore the selective electrocatalytic hydrogenation of lignin monomers to methoxylated chemicals, of particular interest, when powered by renewable electricity. Prior studies, while advancing the field rapidly, have so far lacked the needed selectivity: when hydrogenating lignin-derived methoxylated monomers to methoxylated cyclohexanes, the desired methoxy group ($-OCH_3$) has also been reduced. The ternary PtRhAu electrocatalysts developed herein selectively hydrogenate lignin monomers to methoxylated cyclohexanes—molecules with uses in pharmaceutics. Using X-ray absorption spectroscopy and *in situ* Raman spectroscopy, we find that Rh and Au modulate the electronic structure of Pt and that this modulating steers intermediate energetics on the electrocatalyst surface to facilitate the hydrogenation of lignin monomers and suppress $C-OCH_3$ bond cleavage. As a result, PtRhAu electrocatalysts achieve a record 58% faradaic efficiency (FE) toward 2-methoxycyclohexanol from the lignin monomer guaiacol at 200 mA cm^{-2}, representing a 1.9× advance in FE and a 4× increase in partial current density compared to the highest productivity prior reports. We demonstrate an integrated lignin biorefinery where wood-derived lignin monomers are selectively hydrogenated and funneled to methoxylated 2-methoxy-4-propylcyclohexanol using PtRhAu electrocatalysts. This work offers an opportunity for the sustainable electrocatalytic synthesis of methoxylated pharmaceuticals from renewable biomass.

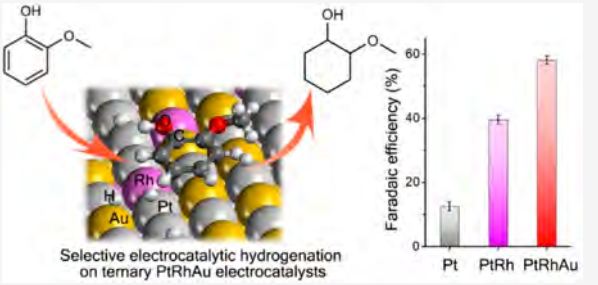

1. INTRODUCTION

The valorization of lignin—an abundant source of renewable organic carbon—into valuable organic chemicals offers to contribute to reducing reliance on fossil resources. Lignin monomers derived from the depolymerization of lignin include methoxylated aromatics[1] that can function as renewable feedstocks[2−7] in the production of methoxylated cyclohexane derivatives used in pharmaceutics[8−10] since their methoxy group has antimicrobial[10,11] and anticancer activity.[12] For example, 2-methoxy-cyclohexanol (2MC, consisting of $-OCH_3$ on cyclohexane ring) is an intermediate of high-value β-lactam antibiotics for human immunodeficiency viruses.[13,14]

Electrocatalytic hydrogenation (ECH) has been widely studied to valorize lignin monomers into cyclohexane derivatives.[15−21] ECH uses an applied potential to produce adsorbed hydrogen on an electrocatalyst surface by splitting water,[22] and this then directly hydrogenates the lignin aromatic monomers to cyclohexane derivatives.[18,20] The ECH approach benefits from mild operating conditions (ambient temperature and pressure), avoids organic solvents, and offers routes to tune product selectivity by controlling potential.[15,18−20,23−25]

Unfortunately, there exists a key difficulty in using ECH to produce methoxylated cyclohexane derivatives from lignin monomers: demethoxylation is thermodynamically favored under cathodic reducing conditions.[15,26−31] For example, guaiacol, a representative lignin-derived aromatic monomer with −OH and $-OCH_3$ groups (Figure 1a), has so far been electrocatalytically reduced to cyclohexanol and cyclohexanone as major products—and with the desired 2MC as only a minor product.[15,30] The demethoxylation reaction dominates[15,28,29,32] because $-OCH_3$ is more prone to reduction than is the −OH

Received: August 9, 2021

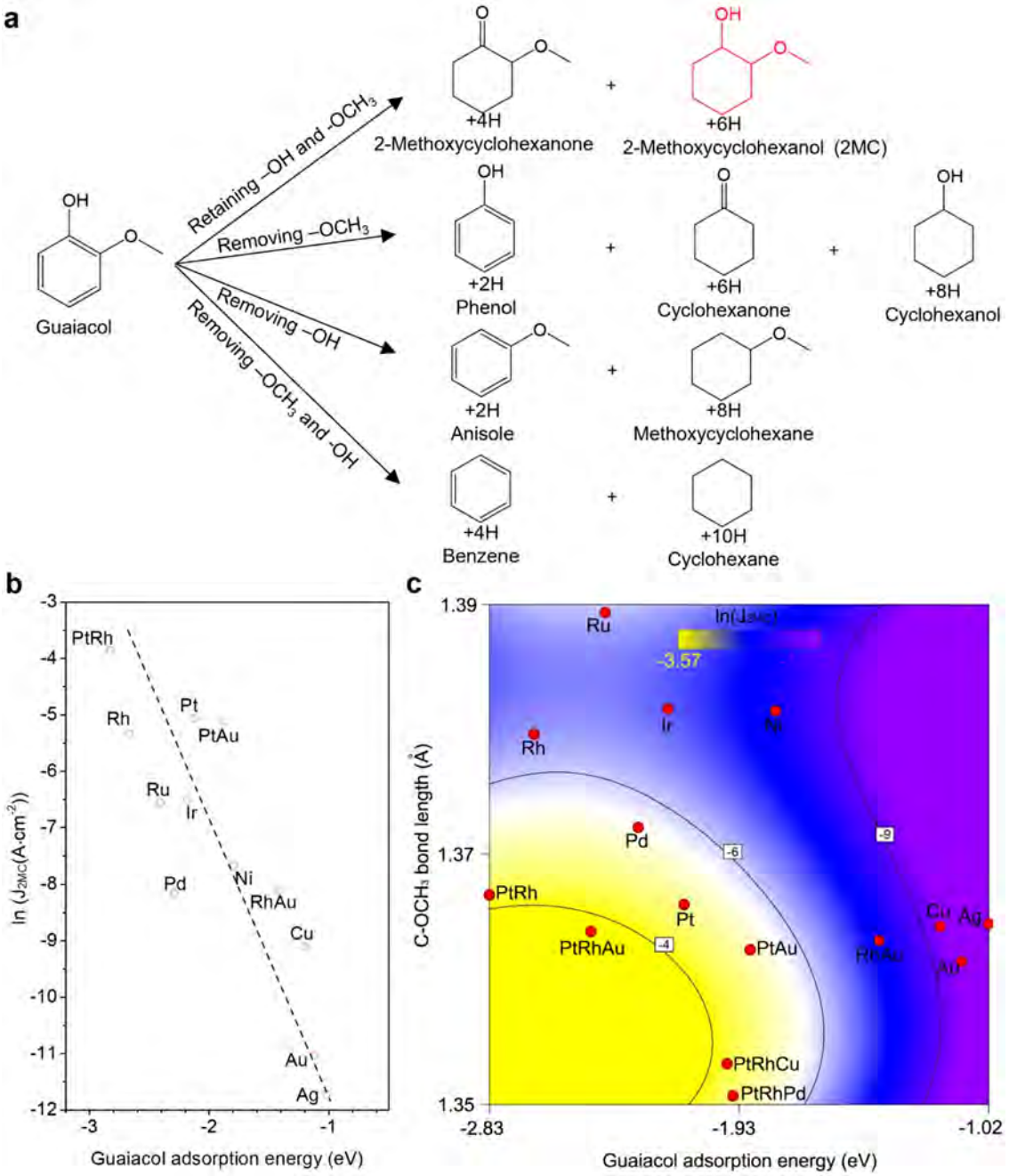

Figure 1. Steering catalyst selectivity toward 2-methoxycyclohexanol (2MC) by tuning guaiacol adsorption energy and C−OCH_3 bond length. (a) Electrocatalytic hydrogenation of guaiacol and potential products. 2MC is the target structure in red. (b) Correlation between guaiacol adsorption energy and electrocatalytic hydrogenation performance ($\ln(J_{2MC})$). (c) Interaction between guaiacol adsorption energy (estimated uncertainty 0.1 eV) and C−OCH_3 bond length (estimated uncertainty 0.005 Å) in determining electrocatalytic hydrogenation performance ($\ln(J_{2MC})$) (standard deviation in Table S1).

group.[33] As a result, high FE and current density toward 2MC are challenging to achieve. A more efficient ECH route for 2MC is thus needed.

We therefore sought a route to develop electrocatalysts to facilitate the hydrogenation of the lignin monomer guaiacol while suppressing demethoxylation. Preliminary computational studies allowed us to screen various single metal electrocatalysts, and from these we found that Pt and Rh possess high guaiacol adsorption energy, suggesting ECH performance greater than that of reference single metal electrocatalysts. We then selected metals (e.g., Au, Pd, and Cu) that would modulate the electronic properties of Pt and Rh to shorten the C−OCH_3 bond of adsorbed guaiacol on the electrocatalyst surface, addressing the energetics of key reaction intermediates to inhibit demethoxylation, thus promoting 2MC production. Using the resultant electrocatalysts, we selectively hydrogenated guaiacol to a methoxylated cyclohexane derivative 2MC with a high FE and current density at ambient temperature and pressure. We report a pilot integrated lignin biorefinery that allows us to obtain methoxylated cyclohexane derivatives directly from wood biomass, showcasing the

https://doi.org/10.1021/jacs.1c08348
J. Am. Chem. Soc. XXXX, XXX, XXX−XXX

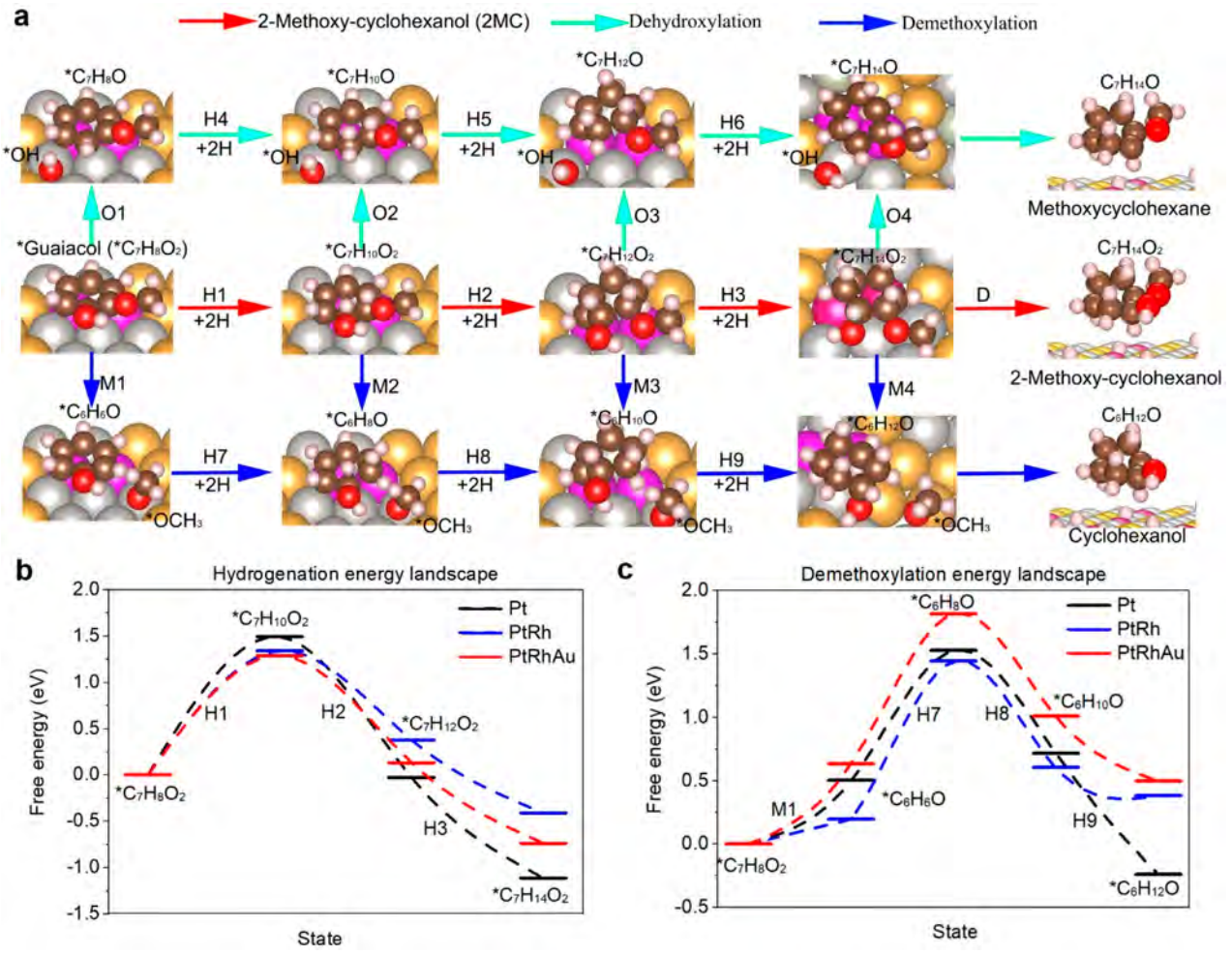

Figure 2. DFT calculations on 2-methoxycyclohexanol (2MC) formation and suppression of demethoxylation. (a) Geometries of reactants and intermediates on PtRhAu catalyst surface to produce 2MC and two competing reactions. The reaction pathway to 2MC: H1−H3, the addition of hydrogen to the aromatic ring, D, desorption. The competing reaction steps O1−O4, M1−M4, and H4−H9 represent dihydroxylation, demethoxylation, and hydrogenation, respectively. Gray, yellow, purple, brown, red, and pink spheres represent Pt, Au, Rh, C, O, and H atoms, respectively. (b) Free energy profiles for electrocatalytic hydrogenation of guaiacol to 2MC pathway H1−H3 as illustrated in (a). (c) Free energy profiles for demethoxylation pathway M1−H7−H8−H9 as illustrated in (a).

selective hydrogenation and funneling of mixed lignin monophenolics to alkylated 2MC.

2. RESULTS AND DISCUSSION

Density Functional Theory (DFT) Calculations. We began by calculating the guaiacol adsorption energy ($E_{ad\text{-}G}$) on various single-metal electrocatalysts (Pt, Rh, Au, Ag, Ni, Pd, Cu, Ru, and Ir) by using a previously reported approach[33−35] (Figure 1b, Figures S1 and S2, and Tables S1 and S2). This preliminary study highlighted Pt ($E_{ad\text{-}G}$ = 2.12 eV) and Rh ($E_{ad\text{-}G}$ = 2.67 eV) as potential candidates due to their high $E_{ad\text{-}G}$ (Figure 1b). This motivated us to conduct preliminary experiments to obtain partial current densities toward 2MC (J_{2MC}) on Pt, Rh, and other single-metal electrocatalysts. By correlating $E_{ad\text{-}G}$ with the measured J_{2MC}, we found that an increase in $E_{ad\text{-}G}$ is linearly correlated to an increase in $\ln(J_{2MC})$ (Figure 1b). This accords with a picture in which increased $E_{ad\text{-}G}$ is linked to an increase in guaiacol concentration on the catalyst surface. We then considered binary systems such as PtRh, PtAu, and RhAu alloys to increase the $E_{ad\text{-}G}$ further. DFT calculations predict that PtRh would have a stronger $E_{ad\text{-}G}$ compared to PtAu and RhAu, and thus an increased catalytic activity toward 2MC (Figure 1b). This prediction is further confirmed by the measured activity reported via J_{2MC}.

We then sought to suppress the reduction of the C−OCH_3 bond that is more prone to scission than C−OH (Figure S4). We reduced the C−OCH_3 bond length on the catalyst surface by modulating PtRh by using a third transition metal. Our preliminary DFT calculations on single-metal catalysts indicate that Au (with an adsorbed guaiacol C−OCH_3 bond length of 1.360 Å) has a stronger ability to localize the σ-electron and reduce the C−OCH_3 bond length compared to Pt (C−OCH_3 bond length = 1.365 Å), Rh (C−OCH_3 bond length = 1.378 Å), and other selected metals (Table S1). We predicted, therefore that it would kinetically suppress the detachment of the −OCH_3 group. Combining the above two descriptors ($E_{ad\text{-}G}$ and C−OCH_3 bond length), we obtained a contour diagram (Figure 1c) that suggests improved performance using ternary PtRhAu catalysts, also consistent with the increased J_{2MC}. PtRhAu catalysts offer both increased $E_{ad\text{-}G}$ and shorter C−OCH_3 bond lengths; in contrast, PtRhPd and PtRhCu show no increase in J_{2MC}, a finding we assign to weaker $E_{ad\text{-}G}$ even though they have shorter C−OCH_3 bond lengths.

https://doi.org/10.1021/jacs.1c08348
J. Am. Chem. Soc. XXXX, XXX, XXX−XXX

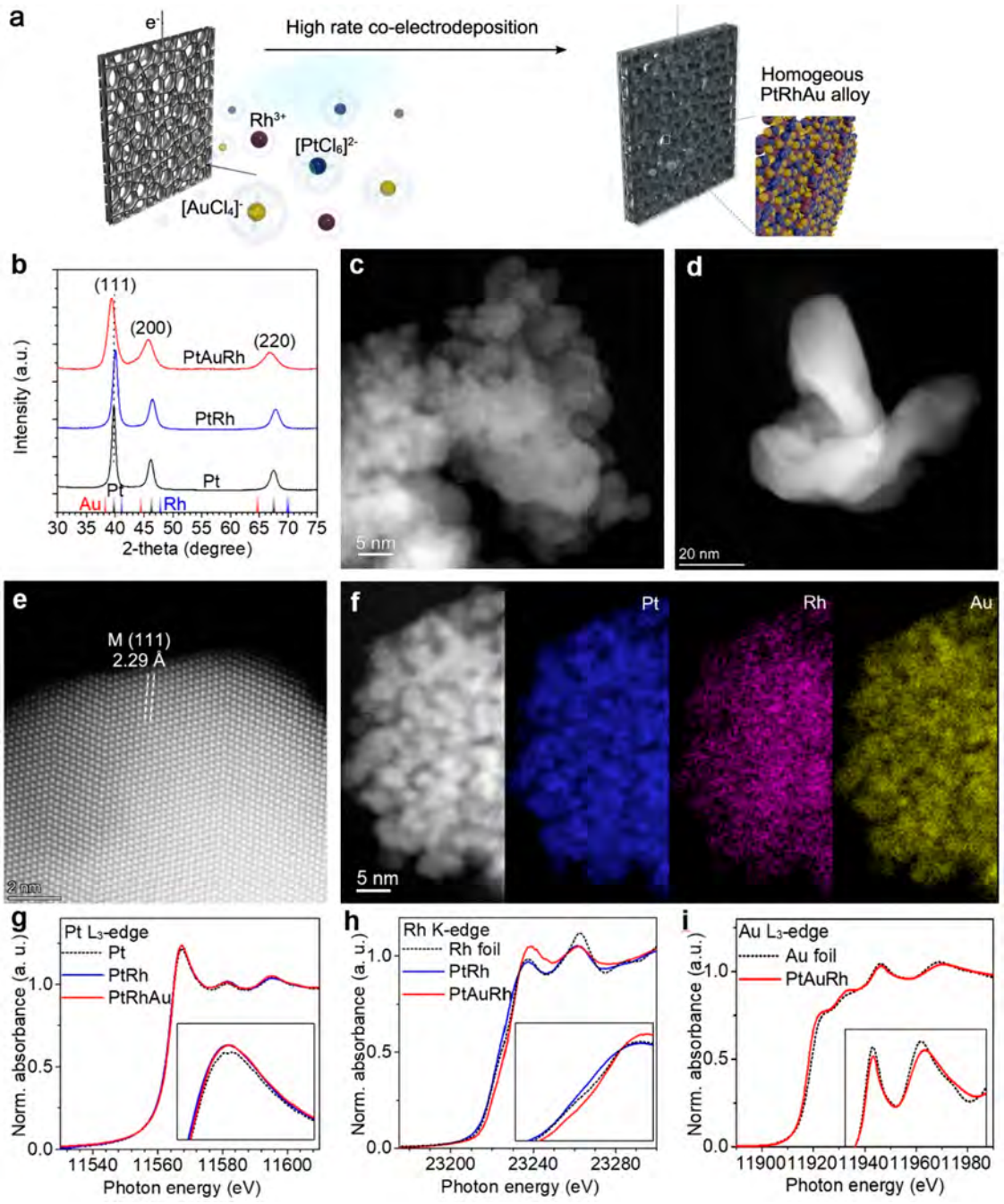

Figure 3. Electrocatalyst synthesis and structural characterization. (a) Schematic illustrating the fabrication of PtRhAu catalysts coated on carbon felt. (b) Synchrotron XRD spectra of Pt, PtRh, and PtRhAu samples, highlighting the peak shift and alloy structure. STEM images of PtRhAu nanoparticles, showing the dendritic morphology (c, d) and the lattice spacing (e). (f) EELS of PtRhAu indicating the substantially homogeneous distribution of Pt, Au, and Rh elements. (g) Pt L_3-edge, (h) Rh K-edge, and (i) Au L_3-edge XAS of PtRhAu, PtRh, Pt, Au, and Rh standards.

With the goal of further understanding the mechanism, we calculated the surface reaction network and the energetics of the intermediates (Figure 2a and Figure S4). The energy profile (Figure 2b) indicates that the rate-determining step along the pathway of adding hydrogen to the aromatic ring is the addition of the first pair of hydrogen atoms. Both PtRh (1.34 eV) and PtRhAu (1.29 eV) catalysts lead to a decrease in hydrogenation energy compared to Pt alone (1.49 eV), indicating a beneficial role of Rh in hydrogenation (Figure 2b). Undesired demethoxylation pathway (Figure 2c) is thermodynamically less favored with PtRhAu catalysts than with pure Pt and PtRh; i.e., Au inhibits demethoxylation and dehydroxylation. Among Pt, PtRh, and PtRhAu, only the ternary PtRhAu catalysts have an ECH pathway (1.29 eV for H1 pathway) that is more favored than the demethoxylation pathway (1.37 eV for M1 + M2 pathways). By comparing five elementary steps—some relating to the activity (adsorption, hydrogenation, and desorption) and others to selectivity (demethoxylation and dehydroxylation)—we concluded that the ternary PtRhAu catalysts show particular promise (Figure S7).

PtRhAu Alloy Catalysts and Structures. We synthesized PtRhAu, Pt, and PtRh using an electrochemical deposition method (Figure 3a) (see the Method section in the Supporting

https://doi.org/10.1021/jacs.1c08348
J. Am. Chem. Soc. XXXX, XXX, XXX−XXX

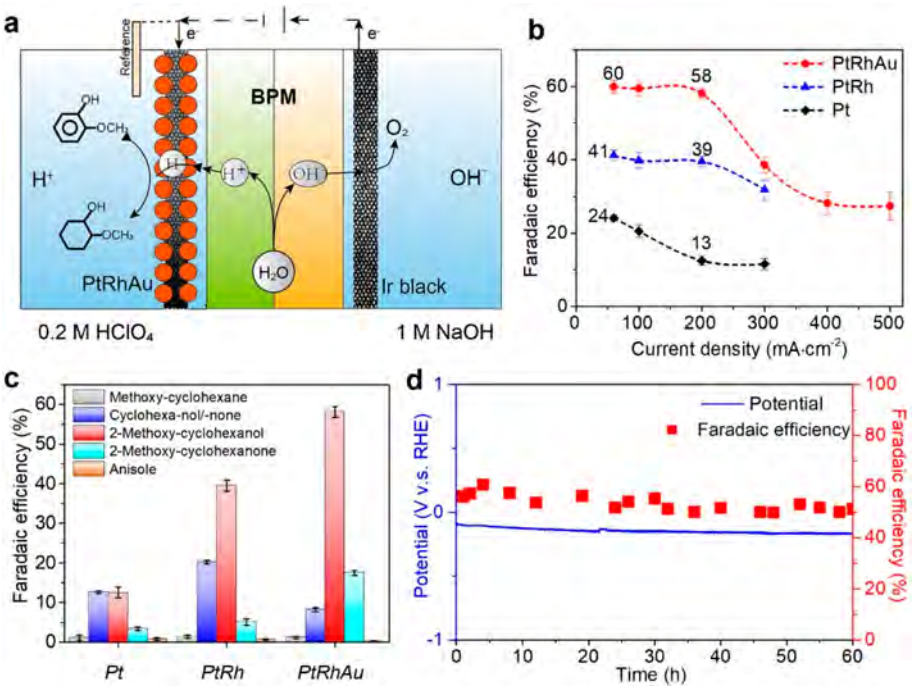

Figure 4. Guaiacol electrocatalytic hydrogenation (ECH). (a) Schematic illustration of a flow-cell system with a bipolar membrane separator. Bipolar membrane consisting of an anion-exchange layer and a cation-exchange layer can disassociate water when a sufficient potential is applied. (b) FE toward 2MC at various current densities for 1 h reaction. (c) FE toward various products on Pt, PtRh, and PtRhAu catalysts at 200 mA cm^{-2} for 1 h reaction. (d) Stable chronoamperometric operation of PtRhAu at a current density of 200 mA cm^{-2} with the optimum FE toward 2MC by using a flow-cell system. Error bars correspond to the standard deviation of three independent measurements. BPM represents the bipolar membrane.

Information). We first optimized the chemical composition of PtRh and PtRhAu catalysts to maximize the FE toward 2MC (Figure S8) and then investigated the nanostructure and morphology of the optimized catalysts. Synchrotron X-ray diffraction (XRD) peaks of PtRh (Figure 3b) shift to higher 2θ values compared to pure Pt, indicating a decreased lattice spacing of PtRh catalyst, while synchrotron XRD peaks of PtRhAu (Figure 3b) shift to lower 2θ values, indicating an increased lattice spacing of PtRhAu. These shifts are attributed to the shorter atomic radius of Rh (1.34 Å) and the larger atomic radius of Au (1.44 Å) compared to Pt (1.39 Å).[36] The changes in lattice spacing indicate the formation of PtRh and PtRhAu alloys. The PtRhAu alloy has a dendritic morphology consisting of nanoparticles with diameters in the range of 5 and 20 nm (Figure 3c,d and Figure S10). The synchrotron XRD peak shifts, along with STEM and HRTEM images, indicate that PtRhAu has a lattice expansion (lattice spacing of 2.29 Å, Figure 3e) compared to Pt (2.26 Å), while PtRh has a lattice contraction (2.24 Å) (Figure S11). We performed electron energy loss spectroscopy (EELS) (Figure 3f) and energy-dispersive X-ray spectroscopy (EDX) (Figure S12) elemental mapping and found a substantially uniform spatial distribution of Pt, Au, and Rh in PtRhAu to within the 0.25 nm spatial resolution of the technique. X-ray photoelectron spectroscopy (XPS) analysis shows an atomic Pt:Rh:Au ratio of 43:9:48 on the surface of the optimized PtRhAu catalysts having the most selective hydrogenation activity (Figure S13), in line with the inductively coupled plasma atomic emission spectroscopy (ICP-AES) analysis (bulk atomic Pt:Rh:Au ratio of 48:8:44).

By tracking changes in X-ray absorption near-edge structure (XANES) (Figures 3g–i) and extended X-ray absorption fine structure (EXAFS) spectra (Figure S14), we examined the local electronic and coordination structure of Pt. The Pt L_3-edge white-line intensity increases and Rh K-edge rising edge shifts to higher photon energy value, while the Au L_3-edge white-line slightly decreases compared to their metallic phase, indicating electron transfer from Pt and Rh to Au. These are consistent with XPS spectra, wherein PtRhAu contains Pt 4f and Rh 3d shifted to a higher binding energy and Au 4f shifted to a lower binding energy[37] (Figure S15). Pt L_3-edge, Au L_3-edge, and Rh K-edge EXAFS spectra for PtRhAu (Figure S14) show slight changes in atomic bonding for Pt and Au atoms and a significant change in atomic bonding for Rh compared to monometallic controls due to alloying.

Electrocatalytic Hydrogenation Performance. We first conducted ECH in a three-electrode H-cell system (Figure S22a) to optimize catalyst composition (Figure S8) and reaction conditions (e.g., pH, temperature, guaiacol concentration, and current density) (Figure S16). We achieved an FE of 47 ± 1% toward 2MC in an H-cell system using the optimized PtRhAu catalyst (a surface Pt:Rh:Au atomic ratio of 43:9:48 determined by XPS (Figure S8)) at an applied current density of 60 mA cm^{-2} (−0.15 V). ^{1}H NMR (Figure S17) and GC-MS (Figure S18) analyses confirm the production of 2MC from guaiacol after 1 h of ECH at 60 mA cm^{-2}. PtRhAu shows superior selectivity toward 2MC at an applied current density of 60 mA cm^{-2} compared to other controls (e.g., Pt, Au, Rh, PtAu, PtRh, and AuRh alloys) (Figure S19). By analyzing the total FE to all organic products and hydrogen (Figure S21), we found that the total measured FE of 85% is lower than 100% in an H-cell equipped with a Nafion 117 membrane. We attribute this to crossover of organics through the Nafion 117 membrane.[38] The bipolar membrane has been reported as a separator showing decreased crossover of organic products.[39]

https://doi.org/10.1021/jacs.1c08348
J. Am. Chem. Soc. XXXX, XXX, XXX−XXX

We, therefore, sought to increase the total measured FE to 96% and the FE to 2MC from 47 ± 1% to 52 ± 1% by replacing the Nafion 117 membrane with the bipolar membrane.

We then sought to increase the FE and current density by using a flow-cell system (Figure 4a and Figure S22c) that lowers electrical resistance and improves mass transport compared to the H-cell system (Figure S22d). The flow-cell system is equipped with a bipolar membrane separator that shows a decreased crossover of organic chemicals (e.g., guaiacol and 2MC) (Figure S23) compared to Nafion 117 membrane.[39,40] PtRhAu in a flow-cell system shows an enhanced FE and current density compared to an H-cell system. The FE toward 2MC achieves 60 ± 2% at a current density of 60 mA cm^{-2} (−0.07 V) and remains at 58 ± 1% at an applied current density of 200 mA cm^{-2} (−0.12 V) (Figure 4b). The FE and partial current density (116 ± 3 mA cm^{-2}) toward 2MC are 1.9× and 4.1× greater than the best prior reports (an FE of 31%[28] and a partial current density of 28 mA cm^{-2},[32] Table S3). The FE decreases significantly at current densities from 300 to 500 mA cm^{-2}: hydrogen evolution reaction dominates at these higher current densities (higher applied reducing potential). PtRhAu catalysts convert 95% of the guaiacol, providing a 76% selectivity toward 2MC at 200 mA cm^{-2} over the course of a 5 h reaction (Figure S24).

Comparing the product distribution of PtRh and Pt (Figure 4c) indicates that incorporation of Rh increases selectivity toward hydrogenated products (e.g., cyclohexanol, cyclohexanone, 2MC, and 2-methoxycyclohexanone), suggesting that Rh promotes the hydrogenation of guaiacol. With the further incorporation of Au, the ternary PtRhAu catalysts enable higher FE toward 2MC and suppress the formation of demethoxylated byproducts (cyclohexanone and cyclohexanol).

We explored the stability of the ternary catalysts by performing ECH of guaiacol. We first investigated the catalyst stability by using *in situ* XAS (Figure S25), suggesting the excellent stability of PtRhAu catalysts during the ECH of guaiacol. The PtRhAu maintains an FE of above 50% toward 2MC at a constant current density of 200 mA cm^{-2} (∼−0.15 V) for 60 h of continuous operation in a flow-cell system (Figure 4d and Figure S26). SEM images (Figure S27), HRTEM, STEM with EDX mapping (Figure S28), and XPS (Figure S29) show that PtRhAu catalysts supported on carbon felt maintain their morphological and compositional features over the course of 60 h of operation.

We conducted a brief techno-economic analysis (TEA) to estimate the plant-gate levelized cost of 2MC from ECH of guaiacol in a flow-cell system (TEA details in the Supporting Information text and Figure S30). The TEA indicates that the plant-gate levelized cost of 2MC depends mainly on current density. The lowest economically feasible current density on PtRhAu electrocatalysts is 5 mA cm^{-2}, indicating that the plant-gate levelized cost of 2MC equals its market price of $431/kg at 5 mA cm^{-2} (Figure S31a). Increasing current density from 5 to 200 mA cm^{-2} lowers the plant-gate levelized cost of 2MC to $24/kg because larger current densities decrease the needed electrode surface area and the associated capital cost (electrolyzer, catalyst, and membrane costs) (Figure S31c). PtRhAu electrocatalysts show the lowest plant-gate levelized cost of 2MC at 200 mA cm^{-1}. However, a further increase in current density beyond 200 mA cm^{-2} slightly increases the plant-gate levelized cost of 2MC, since increasing current density to more than 200 mA cm^{-2} lowers the FE and increases full-cell potential (Figure S31e), which increases the electricity cost.

Mechanistic Investigations. We investigated the ECH mechanism by evaluating reaction intermediates using electrode-potential-dependent *in situ* Raman spectra (Figure 5) and *in situ* infrared reflection−absorption spectroscopy

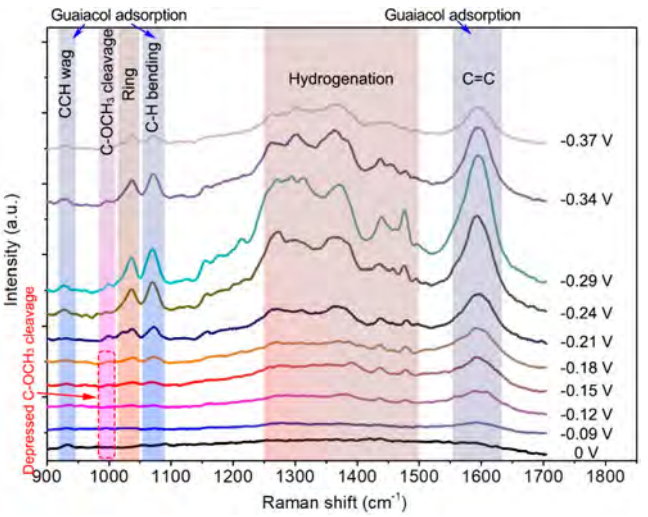

Figure 5. Operando Raman spectra of the electrocatalytic hydrogenation of guaiacol with suppressed demethoxylation on PtRhAu catalysts in 0.2 M electrolyte with 120 mM guaiacol.

(IRRAS). We associate the characteristic peaks from 0 to −0.37 V versus RHE with the ECH of guaiacol. PtRhAu has a wider electrochemical potential window (0 to −0.37 V) compared to Pt (0 to −0.14 V) (Figure S33). The *in situ* Raman spectra of PtRhAu show intensive peaks associated with the guaiacol adsorption (930, 1069, and 1597 cm^{-1})[41,42] and hydrogenation reaction (band between 1250 and 1500 cm^{-1}),[43] indicating favorable adsorption and ECH of guaiacol on the PtRhAu catalyst surface (detailed in Figure S33). Compared to Pt (Figure S33a), the PtRhAu catalyst shows a decreased peak intensity at 997 cm^{-1} (corresponding to the intermediate adsorbed phenol[44]) caused by C−OCH_3 cleavage of guaiacol via demethoxylation pathway M1 (Figure 2a) in a potential range of −0.09 and −0.18 V, indicating the suppression of demethoxylation. In contrast, Pt shows an evident peak at 997 cm^{-1} between −0.06 and −0.14 V (Figure S33b,c). This indicates that the PtRhAu alloy can suppress the C−OCH_3 cleavage in a potential range of −0.09 and −0.18 V. *In situ* IRRAS of PtRhAu (Figure S34) shows intense peaks related to the adsorption and ECH of guaiacol, along with suppressed peak related to C−OCH_3 cleavage, confirming suppressed demethoxylation on PtRhAu catalyst surface.

Integrated Lignin Biorefinery to Produce Methoxylated Cyclohexanes from Wood. We then sought to develop an integrated lignin valorization approach to upgrade wood to a methoxylated cyclohexane derivative 2-methoxy-4-propylcyclohexanol (2M4PC) (**1**) (Figure 6a). Compared to 2MC, 2M4PC has an additional alkyl side-chain that has the potential to control drug delivery in human cells.[45] A lignin-derived monomer with a para-substitution 4-propylguaiacol (4PG) (**2**) was first produced by using a series of aldehyde-assisted fractionation of pinewood, hydrogenolysis, and purification processes (Figure S35a).[46,47] The 4PG was then electrocatalytically hydrogenated by using PtRhAu catalysts in

https://doi.org/10.1021/jacs.1c08348
J. Am. Chem. Soc. XXXX, XXX, XXX−XXX

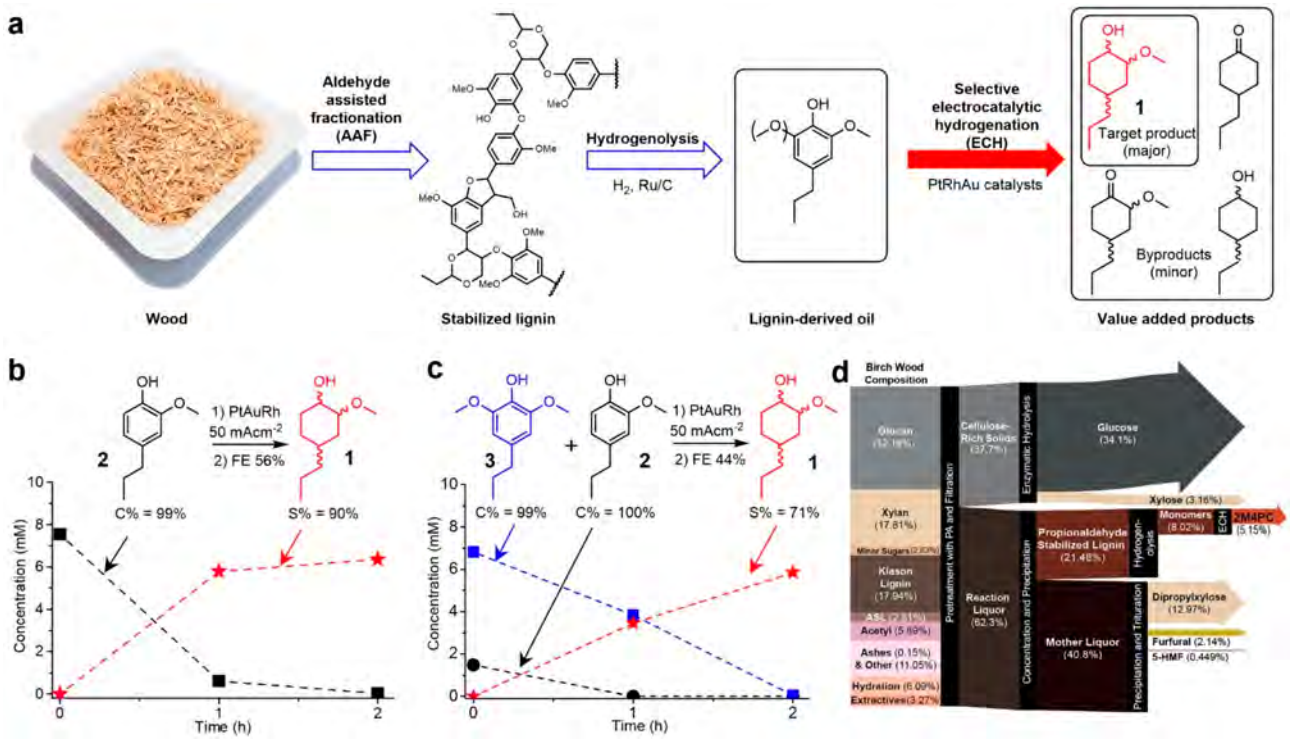

Figure 6. Integrated lignin valorization from wood to a methoxylated product 2-methoxy-4-propylcyclohexanol (2M4PC). (a) Integrated lignin valorization process for high-value 2M4PC from wood. 2M4PC (**1**, red) is the target structure in bold. (b) Concentration evolution of pinewood-derived lignin monomer 4-propylguaiacol (4PG) (**2**, black) and target product 2M4PC (**1**, red), showing an FE at 1 h reaction, conversion rate (*C*%), and product selectivity (*S*%) toward 2MC over 2 h ECH reaction. (c) Concentration evolution of birch-wood-derived lignin oil consisting of 4-propylsyringol (4PS) (**3**, blue) and 4PG (**2**, black) and target product 2M4PC (**1**, red), showing an FE at 1 h reaction, *C*%, and *S*% toward 2MC over 2 h ECH reaction. (d) Mass balances during the propionaldehyde-assisted fractionation of lignocellulosic biomass, as performed on birch wood. All the numbers are provided as weight percentages. The provided weight percentages of the sugars, stabilized sugars, furfural, 5-hydroxymethylfurfural (5-HMF), stabilized lignin, and lignin monomers have been corrected for the mass of the stabilizing group, hydration, dehydration, or hydrogenation to match their initial structure in the native biomass.

a flow-cell system equipped with a bipolar membrane, achieving an FE of 56%, a conversion rate of 99%, and a selectivity of 90% toward the target product **1** at a current density of 50 mA cm^{-2} (Figure 6b and Figure S36). In addition, a less purified lignin-derived oil obtained from birch wood containing a mixture of para-substituted 4PG and 4-propylsyringol (4PS) monomers (Figure 6c and Figure S35b)[46,47] was selectively hydrogenated and funneled to 2M4PC with good overall yield (Figure 6d).

3. CONCLUSIONS

Electrochemical measurements taken together with density functional theory calculations suggest that the Pt catalysts modulated with Rh and Au steer the intermediate energetics on PtRhAu catalysts to increase guaiacol coverage, foster hydrogenation, and suppress demethoxylation. X-ray studies show electron transfer from Pt and Rh to Au and corresponding changes in local coordination structure. *In situ* Raman further reveals key reaction intermediates, indicating roles for Rh and Au in improving the hydrogenation of guaiacol and inhibiting the demethoxylation reaction on PtRhAu catalysts. We report a record FE of 58% and a partial current density of 116 mA cm^{-2} toward a high-value methoxylated cyclohexane derivative 2-methoxycyclohexanol (2MC) from guaiacol. We further achieved an integrated lignin biorefinery from wood, including a syringyl-rich hardwood stream, to a methoxylated cyclohexane derivative, indicating that PtRhAu electrocatalysts selectively hydrogenate and funnel wood-derived lignin monomers to a methoxylated cyclohexane derivative with suppressed demethoxylation reaction. The strategy suggests a means to valorize biomass to methoxylated cyclohexane derivatives.

■ ASSOCIATED CONTENT

Supporting Information

The Supporting Information is available free of charge at https://pubs.acs.org/doi/10.1021/jacs.1c08348.

Detailed information about simulation of nanostructure of PtRhAu catalysts, structure investigation, synchrotron XRD analysis, HRTEM, STEM, EELS, XAS analysis, XPS, ICP-AES, in situ Raman, electrochemical experiments, ^{1}H NMR, stability, liquid product analysis, and the production of lignin oil from wood (PDF)

■ AUTHOR INFORMATION

Corresponding Authors

Jeremy S. Luterbacher − *Laboratory of Sustainable and Catalytic Processing, Institute of Chemicals Sciences and Engineering, Ecole Polytechnique Fédérale de Lausanne (EPFL), Lausanne, VD CH 1015, Switzerland;* orcid.org/0000-0002-0967-0583; Email: jeremy.luterbacher@epfl.ch

Wei Zhao − *Institute for Advanced Study, Shenzhen University, Shenzhen, Guangdong 518060, China;*

https://doi.org/10.1021/jacs.1c08348
J. Am. Chem. Soc. XXXX, XXX, XXX−XXX

orcid.org/0000-0001-5407-6164; Email: weizhao@szu.edu.cn

Edward H. Sargent − *Department of Electrical and Computer Engineering, University of Toronto, Toronto, Ontario M5S 3G4, Canada;* orcid.org/0000-0003-0396-6495; Email: ted.sargent@utoronto.ca

Authors

Tao Peng − *Department of Electrical and Computer Engineering, University of Toronto, Toronto, Ontario M5S 3G4, Canada; Institute for Advanced Study, Shenzhen University, Shenzhen, Guangdong 518060, China;* orcid.org/0000-0001-8517-5368

Taotao Zhuang − *Department of Electrical and Computer Engineering, University of Toronto, Toronto, Ontario M5S 3G4, Canada; Department of Chemistry, University of Science and Technology of China, Hefei, Anhui 230026, China;* orcid.org/0000-0001-5832-8939

Yu Yan − *Department of Electrical and Computer Engineering, University of Toronto, Toronto, Ontario M5S 3G4, Canada*

Jin Qian − *Chemical Sciences Division, Lawrence Berkeley National Laboratory, Berkeley, California 94720, United States;* orcid.org/0000-0002-0162-0477

Graham R. Dick − *Laboratory of Sustainable and Catalytic Processing, Institute of Chemicals Sciences and Engineering, Ecole Polytechnique Fédérale de Lausanne (EPFL), Lausanne, VD CH 1015, Switzerland;* orcid.org/0000-0001-5544-6868

Jean Behaghel de Bueren − *Laboratory of Sustainable and Catalytic Processing, Institute of Chemicals Sciences and Engineering, Ecole Polytechnique Fédérale de Lausanne (EPFL), Lausanne, VD CH 1015, Switzerland;* orcid.org/0000-0003-2246-639X

Sung-Fu Hung − *Department of Electrical and Computer Engineering, University of Toronto, Toronto, Ontario M5S 3G4, Canada;* orcid.org/0000-0002-7423-2723

Yun Zhang − *Institute for Advanced Study, Shenzhen University, Shenzhen, Guangdong 518060, China;* orcid.org/0000-0003-0897-8903

Ziyun Wang − *Department of Electrical and Computer Engineering, University of Toronto, Toronto, Ontario M5S 3G4, Canada;* Present Address: School of Chemical Science, The University of Auckland, Auckland 1010, New Zealand; orcid.org/0000-0002-2817-8367

Joshua Wicks − *Department of Electrical and Computer Engineering, University of Toronto, Toronto, Ontario M5S 3G4, Canada;* orcid.org/0000-0001-7819-1167

F. Pelayo Garcia de Arquer − *Department of Electrical and Computer Engineering, University of Toronto, Toronto, Ontario M5S 3G4, Canada;* orcid.org/0000-0003-2422-6234

Jehad Abed − *Department of Electrical and Computer Engineering, University of Toronto, Toronto, Ontario M5S 3G4, Canada*

Ning Wang − *Department of Electrical and Computer Engineering, University of Toronto, Toronto, Ontario M5S 3G4, Canada;* orcid.org/0000-0002-2589-6881

Armin Sedighian Rasouli − *Department of Electrical and Computer Engineering, University of Toronto, Toronto, Ontario M5S 3G4, Canada;* orcid.org/0000-0002-0807-9468

Geonhui Lee − *Department of Electrical and Computer Engineering, University of Toronto, Toronto, Ontario M5S 3G4, Canada;* orcid.org/0000-0002-9264-7420

Miao Wang − *Institute for Advanced Study, Shenzhen University, Shenzhen, Guangdong 518060, China;* orcid.org/0000-0001-6142-6935

Daping He − *Hubei Engineering Research Center of RF-Microwave Technology and Application, School of Science, Wuhan University of Technology, Wuhan, Hubei 430070, China;* orcid.org/0000-0002-0284-4990

Zhe Wang − *Hubei Engineering Research Center of RF-Microwave Technology and Application, School of Science, Wuhan University of Technology, Wuhan, Hubei 430070, China;* orcid.org/0000-0003-1412-8980

Zhixiu Liang − *Chemistry Division, Brookhaven National Laboratory, Upton, New York 11973, United States*

Liang Song − *Chemistry Division, Brookhaven National Laboratory, Upton, New York 11973, United States*

Xue Wang − *Department of Electrical and Computer Engineering, University of Toronto, Toronto, Ontario M5S 3G4, Canada;* orcid.org/0000-0002-6298-1858

Bin Chen − *Department of Electrical and Computer Engineering, University of Toronto, Toronto, Ontario M5S 3G4, Canada;* orcid.org/0000-0002-2106-7664

Adnan Ozden − *Department of Mechanical and Industrial Engineering, University of Toronto, Toronto, Ontario M5S 3G8, Canada;* orcid.org/0000-0002-6924-1967

Yanwei Lum − *Department of Electrical and Computer Engineering, University of Toronto, Toronto, Ontario M5S 3G4, Canada;* orcid.org/0000-0001-7261-2098

Wan Ru Leow − *Department of Electrical and Computer Engineering, University of Toronto, Toronto, Ontario M5S 3G4, Canada;* orcid.org/0000-0002-8189-4813

Mingchuan Luo − *Department of Electrical and Computer Engineering, University of Toronto, Toronto, Ontario M5S 3G4, Canada;* orcid.org/0000-0001-9772-2154

Debora Motta Meira − *CLS@APS sector 20, Advanced Photon Source, Argonne National Laboratory, Argonne, Illinois 60439, United States; Canadian Light Source Inc., Saskatoon, Saskatchewan S7N 2V3, Canada;* orcid.org/0000-0002-7529-2736

Alexander H. Ip − *Department of Electrical and Computer Engineering, University of Toronto, Toronto, Ontario M5S 3G4, Canada;* orcid.org/0000-0002-4604-4792

Complete contact information is available at: https://pubs.acs.org/10.1021/jacs.1c08348

Author Contributions

T.P., T.Z., Y.Y., and J.Q. contributed equally to this work.

Notes

The authors declare no competing financial interest.

■ ACKNOWLEDGMENTS

The authors thank Cathleen Crudden from the Queen's University and Dr. Yuguang C. Li from the University of Toronto for fruitful discussions. The authors thank Y.-F. Liao for the technical support of synchrotron XRD at the BL-12B2 beamline at SPring-8 (NSRRC). The authors thank Natalie Hamada from the Canadian Centre for Electron Microscopy (CCEM) and Zhi-Yi Hu and Lei Xia from the Nanostructure Research Center (NRC) at the Wuhan University of Technology in China, Brockhouse Institute for Materials

Research, and McMaster University for the STEM and EELS measurement support. This work was partially supported by the Natural Sciences and Engineering Research Council (NSERC) of Canada (Grant RGPIN-2017-06477) and the Canadian Institute for Advanced Research (CIFAR) (Grant FS20-154 APPT.2378). This work was partially supported by the Natural Science Foundation of China (21972096) and the Shenzhen Science and Technology Program (JCYJ20190808150615285). The authors thank D. M. Meira for XAS experiments at the Advanced Photon Source (APS), which is an Office of Science User Facility operated for the U.S. Department of Energy (DOE) Office of Science by Argonne National Laboratory and was supported by the U.S. DOE under Contract DE-AC02-06CH11357, and the Canadian Light Source and its funding partners. The IRRAS experiment was performed at Brookhaven National Laboratory supported by the U.S. Department of Energy, Office of Science, Office of Basic Energy Sciences (BES), Chemical Sciences, Geosciences and Biosciences Division, under Contract DE-SC0012704.

REFERENCES

(1) Cui, T.; Ma, L.; Wang, S.; Ye, C.; Liang, X.; Zhang, Z.; Meng, G.; Zheng, L.; Hu, H.-S.; Zhang, J.; Duan, H.; Wang, D.; Li, Y. Atomically dispersed $Pt-N_3C_1$ sites enabling efficient and selective electrocatalytic C−C bond cleavage in lignin models under ambient conditions. *J. Am. Chem. Soc.* **2021**, *143* (25), 9429−9439.

(2) Schutyser, W.; Renders, T.; Van den Bosch, S.; Koelewijn, S. F.; Beckham, G. T.; Sels, B. F. Chemicals from lignin: An interplay of lignocellulose fractionation, depolymerisation, and upgrading. *Chem. Soc. Rev.* **2018**, *47* (3), 852−908.

(3) Ragauskas, A. J.; Beckham, G. T.; Biddy, M. J.; Chandra, R.; Chen, F.; Davis, M. F.; Davison, B. H.; Dixon, R. A.; Gilna, P.; Keller, M.; Langan, P.; Naskar, A. K.; Saddler, J. N.; Tschaplinski, T. J.; Tuskan, G. A.; Wyman, C. E. Lignin valorization: Improving lignin processing in the biorefinery. *Science* **2014**, *344* (6185), 1246843.

(4) Sun, Z.; Bottari, G.; Afanasenko, A.; Stuart, M. C. A.; Deuss, P. J.; Fridrich, B.; Barta, K. Complete lignocellulose conversion with integrated catalyst recycling yielding valuable aromatics and fuels. *Nat. Catal.* **2018**, *1* (1), 82−92.

(5) Du, Y. P.; Heroguel, F.; Luterbacher, J. S. Slowing the kinetics of alumina sol-gel chemistry for controlled catalyst overcoating and improved catalyst stability and selectivity. *Small* **2018**, *14* (34), e1801733.

(6) Sanderson, K. Lignocellulose: A chewy problem. *Nature* **2011**, *474* (7352), S12−4.

(7) Shuai, L.; Amiri, M. T.; Questell-Santiago, Y. M.; Heroguel, F.; Li, Y.; Kim, H.; Meilan, R.; Chapple, C.; Ralph, J.; Luterbacher, J. S. Formaldehyde stabilization facilitates lignin monomer production during biomass depolymerization. *Science* **2016**, *354* (6310), 329−333.

(8) Fu, J.; Ren, Z.; Bacsa, J.; Musaev, D. G.; Davies, H. M. L. Desymmetrization of cyclohexanes by site- and stereoselective C−H functionalization. *Nature* **2018**, *564* (7736), 395−399.

(9) Corey, E. J.; Cheng, X. M. *The Logic of Chemical Synthesis*; John Wiley & Sons: New York, 1989; Vol. *39*, p 436.

(10) Le Bras, J.; Chatterjee, D.; Muzart, J. A simple one-pot synthesis of *β*-alkoxy alcohols from alkenes. *Tetrahedron Lett.* **2005**, *46* (28), 4741−4743.

(11) Felicetti, T.; Cannalire, R.; Pietrella, D.; Latacz, G.; Lubelska, A.; Manfroni, G.; Barreca, M. L.; Massari, S.; Tabarrini, O.; Kieć-Kononowicz, K.; Schindler, B. D.; Kaatz, G. W.; Cecchetti, V.; Sabatini, S. 2-Phenylquinoline *S. aureus* NorA efflux pump inhibitors: Evaluation of the importance of methoxy group introduction. *J. Med. Chem.* **2018**, *61* (17), 7827−7848.

(12) Valdameri, G.; Gauthier, C.; Terreux, R.; Kachadourian, R.; Day, B. J.; Winnischofer, S. M. B.; Rocha, M. E. M.; Frachet, V.; Ronot, X.; Di Pietro, A.; Boumendjel, A. Investigation of chalcones as selective inhibitors of the breast cancer resistance protein: Critical role of methoxylation in both inhibition potency and cytotoxicity. *J. Med. Chem.* **2012**, *55* (7), 3193−3200.

(13) Truppo, M. D. *Biocatalysis in the Pharmaceutical and Biotechnology Industries*; CRC Press: London, 2007; Vol. *11*, pp 296−296.

(14) *HIV Drugs Global Market Report 2020-30: Covid-19 Implications and Growth*; The Business Research Company, 2020; pp 1−200.

(15) Zhou, Y.; Gao, Y.; Zhong, X.; Jiang, W.; Liang, Y.; Niu, P.; Li, M.; Zhuang, G.; Li, X.; Wang, J. Electrocatalytic upgrading of lignin-derived bio-oil based on surface-engineered PtNiB nanostructure. *Adv. Funct. Mater.* **2019**, *29* (10), 1807651.

(16) Singh, N.; Song, Y.; Gutiérrez, O. Y.; Camaioni, D. M.; Campbell, C. T.; Lercher, J. A. Electrocatalytic hydrogenation of phenol over platinum and rhodium: Unexpected temperature effects resolved. *ACS Catal.* **2016**, *6* (11), 7466−7470.

(17) Coche, L.; Moutet, J. C. Electrocatalytic hydrogenation of organic compounds on carbon electrodes modified by precious metal microparticles in redox active polymer films. *J. Am. Chem. Soc.* **1987**, *109* (22), 6887−6889.

(18) Akhade, S. A.; Singh, N.; Gutierrez, O. Y.; Lopez-Ruiz, J.; Wang, H.; Holladay, J. D.; Liu, Y.; Karkamkar, A.; Weber, R. S.; Padmaperuma, A. B.; Lee, M. S.; Whyatt, G. A.; Elliott, M.; Holladay, J. E.; Male, J. L.; Lercher, J. A.; Rousseau, R.; Glezakou, V. A. Electrocatalytic hydrogenation of biomass-derived organics: A review. *Chem. Rev.* **2020**, *120*, 11370−11419.

(19) Sanyal, U.; Lopez-Ruiz, J.; Padmaperuma, A. B.; Holladay, J.; Gutiérrez, O. Y. Electrocatalytic hydrogenation of oxygenated compounds in aqueous phase. *Org. Process Res. Dev.* **2018**, *22* (12), 1590−1598.

(20) Mohle, S.; Zirbes, M.; Rodrigo, E.; Gieshoff, T.; Wiebe, A.; Waldvogel, S. R. Modern electrochemical aspects for the synthesis of value-added organic products. *Angew. Chem., Int. Ed.* **2018**, *57* (21), 6018−6041.

(21) Cao, Y.; Tang, M.; Li, M.; Deng, J.; Xu, F.; Xie, L.; Wang, Y. In situ synthesis of chitin-derived Rh/N−C cataylsts: Efficient hydrogenation of benzoic acid and derivatives. *ACS Sustainable Chem. Eng.* **2017**, *5* (11), 9894−9902.

(22) Jansonius, R. P.; Kurimoto, A.; Marelli, A. M.; Huang, A.; Sherbo, R. S.; Berlinguette, C. P. Hydrogenation without H_2 using a palladium membrane flow cell. *Cell Rep. Phys. Sci.* **2020**, *1* (7), 100105.

(23) Carneiro, J.; Nikolla, E. Electrochemical conversion of biomass-based oxygenated compounds. *Annu. Rev. Chem. Biomol. Eng.* **2019**, *10*, 85−104.

(24) Song, Y.; Chia, S. H.; Sanyal, U.; Gutiérrez, O. Y.; Lercher, J. A. Integrated catalytic and electrocatalytic conversion of substituted phenols and diaryl ethers. *J. Catal.* **2016**, *344*, 263−272.

(25) Lopez-Ruiz, J. A.; Andrews, E.; Akhade, S. A.; Lee, M.-S.; Koh, K.; Sanyal, U.; Yuk, S. F.; Karkamkar, A. J.; Derewinski, M. A.; Holladay, J.; Glezakou, V.-A.; Rousseau, R.; Gutiérrez, O. Y.; Holladay, J. D. Understanding the role of metal and molecular structure on the electrocatalytic hydrogenation of oxygenated organic compounds. *ACS Catal.* **2019**, *9* (11), 9964−9972.

(26) Liu, X.; An, W.; Wang, Y.; Turner, C. H.; Resasco, D. E. Hydrodeoxygenation of guaiacol over bimetallic Fe-alloyed (Ni, Pt) surfaces: Reaction mechanism, transition-state scaling relations and descriptor for predicting C−O bond scission reactivity. *Catal. Sci. Technol.* **2018**, *8* (8), 2146−2158.

(27) Lam, C. H.; Deng, W.; Lang, L.; Jin, X.; Hu, X.; Wang, Y. Minireview on bio-oil upgrading via electrocatalytic hydrogenation: Connecting biofuel production with renewable power. *Energy Fuels* **2020**, *34* (7), 7915−7928.

(28) Li, Z.; Garedew, M.; Lam, C. H.; Jackson, J. E.; Miller, D. J.; Saffron, C. M. Mild electrocatalytic hydrogenation and hydrodeoxygenation of bio-oil derived phenolic compounds using ruthenium supported on activated carbon cloth. *Green Chem.* **2012**, *14* (9), 2540−2549.

https://doi.org/10.1021/jacs.1c08348
J. Am. Chem. Soc. XXXX, XXX, XXX−XXX

(29) Garedew, M.; Young-Farhat, D.; Jackson, J. E.; Saffron, C. M. Electrocatalytic upgrading of phenolic compounds observed after lignin pyrolysis. *ACS Sustainable Chem. Eng.* **2019**, *7* (9), 8375−8386.
(30) Lam, C. H.; Lowe, C. B.; Li, Z.; Longe, K. N.; Rayburn, J. T.; Caldwell, M. A.; Houdek, C. E.; Maguire, J. B.; Saffron, C. M.; Miller, D. J.; Jackson, J. E. Electrocatalytic upgrading of model lignin monomers with earth abundant metal electrodes. *Green Chem.* **2015**, *17* (1), 601−609.
(31) Gandhi, M.; Rajagopal, D.; Senthil Kumar, A. Facile electrochemical demethylation of 2-methoxyphenol to surface-confined catechol on the MWCNT and its efficient electrocatalytic hydrazine oxidation and sensing applications. *ACS Omega* **2020**, *5* (26), 16208−16219.
(32) Liu, W.; You, W.; Gong, Y.; Deng, Y. High-efficiency electrochemical hydrodeoxygenation of bio-phenols to hydrocarbon fuels by a superacid-noble metal particle dual-catalyst system. *Energy Environ. Sci.* **2020**, *13* (3), 917−927.
(33) Lu, J.; Behtash, S.; Mamun, O.; Heyden, A. Theoretical investigation of the reaction mechanism of the guaiacol hydrogenation over a Pt(111) catalyst. *ACS Catal.* **2015**, *5* (4), 2423−2435.
(34) Réocreux, R.; Huynh, M.; Michel, C.; Sautet, P. Controlling the adsorption of aromatic compounds on pt(111) with oxygenate substituents: From DFT to simple molecular descriptors. *J. Phys. Chem. Lett.* **2016**, *7* (11), 2074−2079.
(35) Réocreux, R.; Ould Hamou, C. A.; Michel, C.; Giorgi, J. B.; Sautet, P. Decomposition mechanism of anisole on Pt(111): Combining single-crystal experiments and first-principles calculations. *ACS Catal.* **2016**, *6* (12), 8166−8178.
(36) Bond, G. C. Periodic variations in the catalytic properties of metals. *Platinum Met. Rev.* **1968**, *12* (3), 100−105.
(37) Wang, P.; Zhou, F.; Wang, Z.; Lai, C.; Han, X. Substrate-induced assembly of PtAu alloy nanostructures at choline functionalized monolayer interface for nitrite sensing. *J. Electroanal. Chem.* **2015**, *750*, 36−42.
(38) Song, S.; Zhou, W.; Tian, J.; Cai, R.; Sun, G.; Xin, Q.; Kontou, S.; Tsiakaras, P. Ethanol crossover phenomena and its influence on the performance of DEFC. *J. Power Sources* **2005**, *145* (2), 266−271.
(39) Li, Y. C.; Yan, Z.; Hitt, J.; Wycisk, R.; Pintauro, P. N.; Mallouk, T. E. Bipolar membranes inhibit product crossover in CO_2 electrolysis cells. *Adv. Sustain. Syst.* **2018**, *2* (4), 1700187.
(40) Oener, S. Z.; Foster, M. J.; Boettcher, S. W. Accelerating water dissociation in bipolar membranes and for electrocatalysis. *Science* **2020**, *369*, 1099−1103.
(41) Verma, V. N.; Nair, K. P. R.; Rai, D. K. Vibrational spectra and thermodynamic functions of the three isomeric methoxyphenols. *Isr. J. Chem.* **1970**, *8* (5), 777−789.
(42) Agarwal, U. P.; McSweeny, J. D.; Ralph, S. A. FT−Raman investigation of milled-wood lignins: Softwood, hardwood, and chemically modified black spruce lignins. *J. Wood Chem. Technol.* **2011**, *31* (4), 324−344.
(43) Neelakantan, P. The Raman spectrum of cyclohexanol. *Proc. - Indian Acad. Sci., Sect. A* **1963**, *57* (2), 94−102.
(44) Johnson, C. R.; Ludwig, M.; Asher, S. A. Ultraviolet resonance Raman characterization of photochemical transients of phenol, tyrosine, and tryptophan. *J. Am. Chem. Soc.* **1986**, *108* (5), 905−912.
(45) Stanisic, D.; Costa, A. F.; Cruz, G.; Durán, N.; Tasic, L. Applications of flavonoids, with an emphasis on hesperidin, as anticancer prodrugs: Phytotherapy as an alternative to chemotherapy. In *Studies in Natural Products Chemistry*; Atta-ur-Rahman, Ed.; Elsevier: 2018; Vol. *58*, pp 161−212.
(46) Abu-Omar, M. M.; Barta, K.; Beckham, G. T.; Luterbacher, J.; Ralph, J.; Rinaldi, R.; Roman-Leshkov, Y.; Samec, J.; Sels, B.; Wang, F. Guidelines for performing lignin-first biorefining. *Energy Environ. Sci.* **2021**, *14* (1), 262−292.
(47) Talebi Amiri, M.; Dick, G. R.; Questell-Santiago, Y. M.; Luterbacher, J. S. Fractionation of lignocellulosic biomass to produce uncondensed aldehyde-stabilized lignin. *Nat. Protoc.* **2019**, *14* (3), 921−954.

https://doi.org/10.1021/jacs.1c08348
J. Am. Chem. Soc. XXXX, XXX, XXX−XXX